Electrochimica Acta, Vol. 38, No. 9, pp. 1259–1267, 1993
Printed in Great Britain.

0013-4686/93 $6.00 + 0.00

RAMSDELLITE-MnO_2 FOR LITHIUM BATTERIES: THE RAMSDELLITE TO SPINEL TRANSFORMATION

M. M. THACKERAY,*† M. H. ROSSOUW,† R. J. GUMMOW,† D. C. LILES,† K. PEARCE,† A. DE KOCK,† W. I. F. DAVID‡ and S. HULL‡

† Division of Materials Science and Technology, CSIR, P.O. Box 395, Pretoria 0001, South Africa
‡ Rutherford Appleton Laboratory, Chilton, Didcot, Oxfordshire OX11 0QX, U.K.

(*Received* 2 *September* 1992)

Abstract—A pure and highly crytalline form of ramsdellite-MnO_2 has been synthesized by acid treatment of the spinels $LiMn_2O_4$ and $Li_2Mn_4O_9$ at 95°C. Although the ramsdellite–MnO_2 framework remains intact on lithiation at 70°C, the hexagonally-close-packed oxygen array buckles towards a cubic-close-packed structure to accommodate the inserted lithium ions. The reaction is reversible but the instability of the structure on cycling limits the utility of ramsdellite-MnO_2 as a rechargeable electrode in lithium cells. The ramsdellite structure can be stabilized by reaction with LiOH or $LiNO_3$ at 300–400°C; this reaction, which displaces manganese ions from the MnO_2 framework into interstitial octahedral sites generates spinel-related domains that coexist with the lithiated ramsdellite phase. At 300°C, under vacuum, the lithiated ramsdellite phase $Li_{0.5}MnO_2$ transforms to the spinel $LiMn_2O_4$; at 300–400°C, in air, it oxidizes slowly and transforms to a defect spinel $LiMn_2O_{4+\delta}$ ($0 < \delta \leqslant 0.5$) via an intermediate compound. A mechanism for the ramsdellite–spinel transition is proposed.

Key words: ramsdellite, spinel, manganese dioxide, structure, lithium batteries.

INTRODUCTION

The advent of lithium battery technology has led to the investigation of many of the polymorphs of manganese dioxide as possible cathode materials for rechargeable cells. The materials include:

1. α-MnO_2 (hollandite-type structure)[1–3];
2. γ-MnO_2 (intergrowth of rutile- and ramsdellite-type structures)[4, 5];
3. δ-MnO_2 (layered structures)[6, 7];
4. λ-MnO_2 (spinel-type structure)[8–10].

The structural and electrochemical properties of these materials have been reported widely over several years; they have been made either in pure form or stabilized with lithium. Examples of the lithium-doped materials are the defect spinel $Li_2Mn_4O_9$ ($Li_2O \cdot 4MnO_2$)[11] and "CDMO" products that are synthesized typically by the reaction of LiOH (or $LiNO_3$) with γ-MnO_2 using a Li:Mn ratio of 3:7 at 370°C[12, 13].

The best known MnO_2 polymorph used by the battery industry is γ-MnO_2; it is synthesized either chemically (CMD) or electrolytically (EMD). In Zn/MnO_2 cells it has been demonstrated by neutron-diffraction that protons are inserted into the ramsdellite domains during discharge to form α-MnOOH (groutite)[14, 15]. On the other hand, proton insertion into the rutile-MnO_2 domains causes a transformation to a $Mn(OH)_2$ (pyrochroite) product which has a layered structure. It is believed that the structural incompatibility between groutite and pyrochroite limits the rechargeability of γ-MnO_2 electrodes in aqueous cells.

In Li/γ-MnO_2 cells it is generally acknowledged that discharge occurs predominantly by lithium insertion into the (2 × 1) channels of the ramsdellite domains. The β-MnO_2 domains can only accommodate 0.2 Li^+ ions in the (1 × 1) channels[16]; at higher lithium loadings β-MnO_2 transforms to the $[Mn_2]O_4$ spinel framework[17]. Therefore, because the β-MnO_2 domains in γ-MnO_2 structures appear to have a negative impact on the operation of both zinc and lithium cells, it seemed advantageous to prepare a pure ramsdellite phase to enhance the performance of these cells.

In this paper the synthesis and structural characterization of ramsdellite-MnO_2 (hereafter referred to as R-MnO_2 for convenience) and several lithiated derivatives are described. The electrochemical properties of R-MnO_2 have been evaluated in lithium cells. The results of these studies shed further light on the mechanisms by which Li/γ-MnO_2 cells operate.

EXPERIMENTAL

R-MnO_2 was prepared by reaction of the spinels $LiMn_2O_4$ and $Li_2Mn_4O_9$ in 2.5 M H_2SO_4 at 95°C for 24 h. The spinel precursors were synthesised by solid state reaction of Li_2CO_3 and $MnCO_3$ in air at 750 and 400°C. The resulting R-MnO_2 products were washed in water and dehydrated at 200°C prior to chemical and electrochemical lithiation.

* Author to whom correspondence should be addressed.

Chemical lithiation of R-MnO_2 was achieved by two methods:

1. $Li_{0.3}MnO_2$, $Li_{0.5}MnO_2$ and $Li_{0.9}MnO_2$ were prepared by reacting R-MnO_2 with a solution of LiI in acetonitrile at 70°C for 5 h. A stoichiometric quantity of LiI dissolved in 25 ml of acetonitrile was used for the preparation of $Li_{0.3}MnO_2$ and $Li_{0.5}MnO_2$, whereas a three-times excess of LiI was used for $Li_{0.9}MnO_2$.

2. Two lithiated R-MnO_2 products were prepared by reaction of R-MnO_2 with $LiNO_3$ in a 7:3 molar ratio at 300 and 380°C. The reactions were carried out in air for 20 h.

The lithium and manganese contents in the individual samples were determined by atomic absorption analyses. X-ray diffraction data were collected on a Rigaku powder diffractometer with CuKα radiation, monochromated by a graphite crystal. Time-of-flight neutron diffraction data were collected on the Polaris diffractometer at the Rutherford Appleton Laboratory (U.K.). Structures of R-MnO_2 and lithiated products were refined either with X-ray data using the Wiles, Young and Sakthivel profile refinement program DBW 3.2S as adapted by Schneider[18], or with neutron data using the programs of the Cambridge Crystallographic Subroutine Library (CCSL)[19] and software developed by David and Ibberson[20]. Electrochemical data were collected from flooded electrolyte, prismatic cells. Lithium foil compacted onto nickel gauze was used for both the anode and reference electrodes. The cathode contained typically 25 mg of R-MnO_2 intimately mixed with 20wt% teflon acetylene black (TAB) compacted onto a nickel gauze disc, 1 cm in diameter. In the TAB mixture the ratio of teflon:acetylene black was 1:2. The electrolyte was a 1 M solution of $LiClO_4$ in propylene carbonate or propylene carbonate:dimethoxyethane (1:1 volumetric ratio). Cells were discharged at 0.4 mA and charged at 0.2 mA. Open-circuit voltage readings were recorded at regular intervals allowing a 72 h equilibration time at each point. Cyclic voltammetry data were recorded from similar cells; a scan speed of 0.2 mV s^{-1} was employed in these experiments.

RESULTS AND DISCUSSION

Structural characterization of Li_xMnO_2 ($0 \leqslant x \leqslant 0.9$)

The powder X-ray diffraction patterns of R-MnO_2 and three lithiated derivatives $Li_{0.3}MnO_2$, $Li_{0.5}MnO_2$ and $Li_{0.9}MnO_2$ obtained by reaction with LiI at 70°C are given in Fig. 1a–d. Lithiation

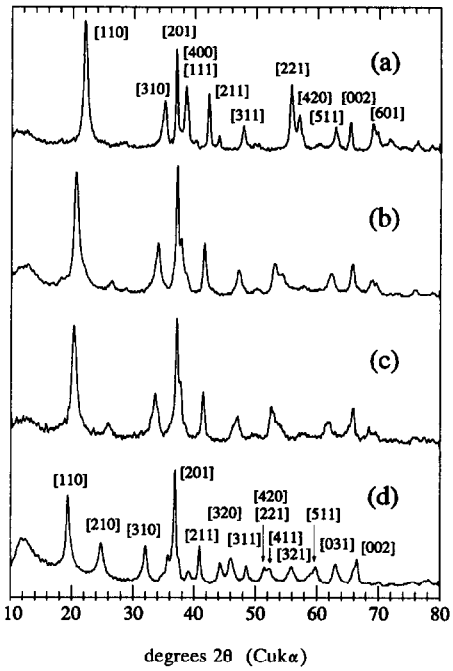

Fig. 1. Powder X-ray diffraction patterns of: (a) R-MnO_2; (b) $Li_{0.3}MnO_2$; (c) $Li_{0.5}MnO_2$; and (d) $Li_{0.9}MnO_2$.

results in single-phase Li_xMnO_2 products, the X-ray patterns of which could be indexed to an orthorhombic unit cell with the same symmetry as the parent R-MnO_2 (Pnam). The unit cell expands significantly on lithiation from 11.1% in $Li_{0.3}MnO_2$ to a massive 21.5% in $Li_{0.9}MnO_2$. The increase in cell volume is a result of large increases in the *a* and *b* lattice parameters; the *c* parameter is effectively unchanged by lithiation (Table 1). Atomic parameters of the various products are listed in Table 2.

The structure of R-MnO_2 was determined by profile refinement of neutron data (Fig. 2) and X-ray data (Fig. 3). The lattice parameters derived from these refinements ($a = 9.372$ Å, $b = 4.471$ Å, $c = 2.851$ Å) are in agreement with those reported for natural ramsdellite-MnO_2[21]. A [001] Fourier projection of the neutron data, clearly shows the positions of the Mn and O atoms (Fig. 4a). A difference Fourier projection (Fig. 4b) indicates some residual scattering at the Mn and O positions; there is no evidence of scattering from the interstitial octahedral sites in the (2 × 1) channels of the structure. It was therefore concluded that in this particular sample there was an insignificant concentration of β-MnO_2 (rutile) domains in the R-MnO_2 structure.

Table 1. Lattice parameters of ramsdellite-related Li_xMnO_2 compounds (Space Group Pnam)

	R-MnO_2 (neutron data)	R-MnO_2 (X-ray data)	$Li_{0.3}MnO_2$	$Li_{0.5}MnO_2$	$Li_{0.9}MnO_2$
a (Å)	9.351 (1)	9.372 (2)	9.446 (5)	9.501 (4)	9.910 (5)
b (Å)	4.449 (1)	4.471 (1)	4.932 (4)	4.985 (3)	5.208 (3)
c (Å)	2.845 (1)	2.851 (1)	2.850 (1)	2.841 (1)	2.812 (1)
Unit cell volume (Å^3)	118.4 (1)	119.5 (1)	132.8 (2)	134.6 (2)	145.1 (2)
Volume expansion	—	—	11.1%	13.7%	21.5%

Table 2. Atomic parameters of R-MnO_2 and lithiated derivatives (Space Group Pnam)

	x	y	z	B_{11}	B_{22}	B_{33}	B_{12}
R-MnO_2 (neutron data)							
Mn	0.1265 (16)	0.0160 (29)	0.25	1.44	1.13	1.83	0.18
O(1)	0.2841 (11)	0.2941 (18)	0.25	2.41	1.58	2.02	−1.78
O(2)	−0.0380 (15)	−0.2340 (6)	0.25	0.67	2.49	0.09	0.28
R-MnO_2 (X-ray data)							
Mn	0.1333 (6)	0.0160 (15)	0.25				
O(1)	0.2866 (15)	0.2838 (22)	0.25		Overall B = 0.45 (7)		
O(2)	−0.0339 (15)	−0.1992 (24)	0.25				
$Li_{0.3}MnO_2$							
Mn	0.1326 (7)	0.0453 (14)	0.25				
O(1)	0.2755 (17)	0.3545 (25)	0.25		Overall B = 2.46 (14)		
O(2)	0.0089 (15)	−0.2072 (26)	0.25				
$Li_{0.5}MnO_2$							
Mn	0.1395 (5)	0.0498 (10)	0.25				
O(1)	0.2607 (16)	0.3714 (26)	0.25		Overall B = 1.16 (13)		
O(2)	0.0051 (13)	−0.2276 (27)	0.25				
$Li_{0.9}MnO_2$							
Mn	0.1280 (7)	0.0958 (8)	0.25				
O(1)	0.2649 (13)	0.4271 (24)	0.25		Overall B = 2.05 (20)		
O(2)	0.0107 (13)	−0.2437 (22)	0.25				

The structure of R-MnO_2 is shown in Fig. 5a. The structures of the lithiated products $Li_{0.3}MnO_2$, $Li_{0.5}MnO_2$ and $Li_{0.9}MnO_2$ as determined by profile refinements of X-ray data are shown in Fig. 5b–d. These refinements demonstrate that at 70°C the R-MnO_2 framework remains intact over the whole compositional range of Li_xMnO_2 ($0 \leqslant x \leqslant 0.9$). Although it was not possible to determine accurately the positions of the Li^+ ions in the structures from the X-ray data, a small amount of scattering was detected from the interstitial octahedral sites of the R-MnO_2 framework (Fig. 5b–d). Lithium insertion into the hexagonally-close-packed oxygen array of R-MnO_2 causes a shear of the (2 × 1) ramsdellite blocks and a buckling of the structure in response to an increase in electrostatic interactions between lithium and manganese ions in face-shared octahedra. The shear transforms the R-MnO_2 structure, in which the close-packed oxygen layers are initially parallel to the *ac* plane, to a lithiated structure in which the close-packing of the oxygens develops parallel to the *bc* plane. In $Li_{0.9}MnO_2$ the layering adopts a sequence ABACABAC which is a combination of hexagonal-close-packing (ABA) and cubic-close-packing (BAC) (Fig. 5d).

The reaction of R-MnO_2 *with* $LiNO_3$ *at* 300 *and* 380°C

It is now well known that lithiated γ-MnO_2 products formed by the reaction of LiOH or $LiNO_3$ with CMD or EMD at 350–420°C offer superior cycling properties in rechargeable lithium cells compared to conventionally heat-treated CMD and EMD electrodes. The lithium-stabilized materials are

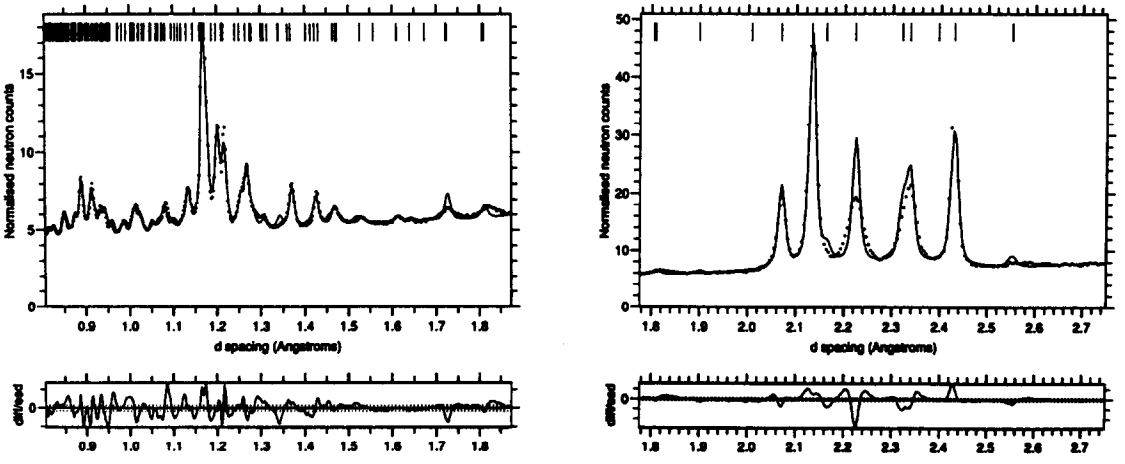

Fig. 2. The observed and calculated neutron diffraction patterns of R-MnO_2.

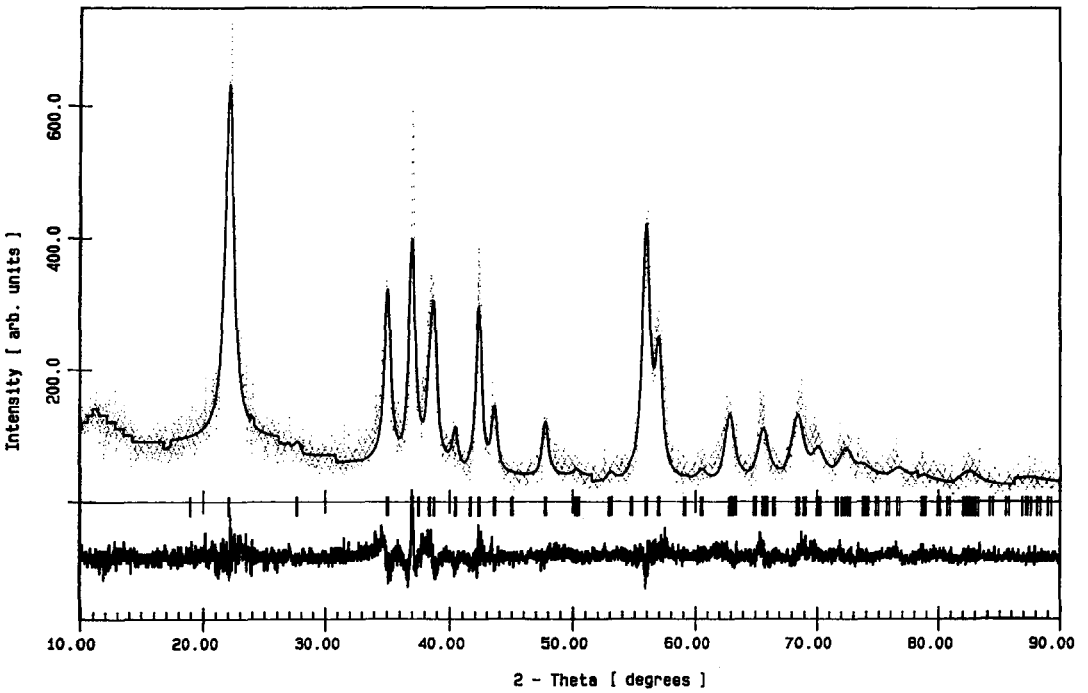

Fig. 3. The observed and calculated X-ray diffraction patterns of R-MnO_2.

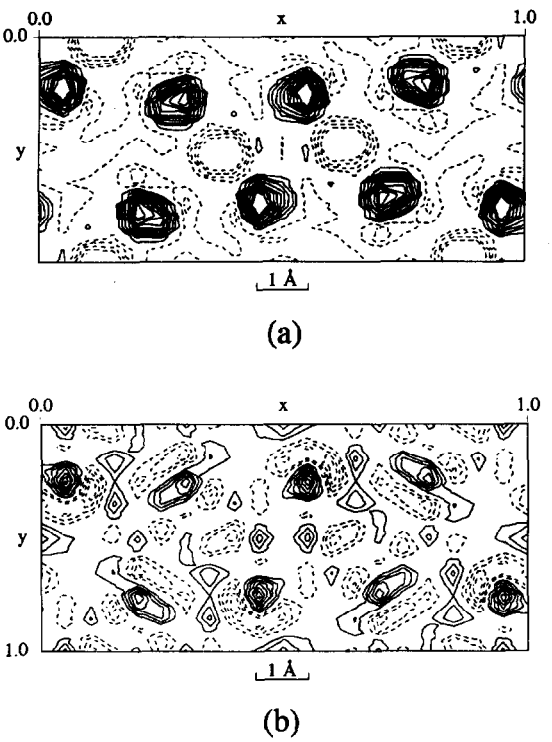

Fig. 4. (a) A Fourier projection of the R-MnO_2 unit cell onto the [001] plane from neutron-diffraction data showing the positions of the Mn atoms (dashed, negative contours) and O atoms (solid, positive contours). (b) A difference Fourier projection of R-MnO_2 showing residual scattering from the Mn and O sites but negligible scattering from the interstitial octahedral sites.

now generally known as CDMO materials after Sanyo[12]. An optimum performance is obtained when CMD or EMD (sometimes pretreated with HNO_3 or H_2O_2) is reacted with $LiNO_3$ or LiOH in a 7:3 molar ratio at 370°C[22–25]. The nature of this product has been interpreted in several ways:

1. as a single-phase γ-related Li_xMnO_2 product in which x varies between 0.2 and 0.3[22];
2. as a composite electrode containing domains of a lithiated γ-MnO_2 phase and Li_2MnO_3[12, 13]; or
3. as an intergrown structure containing domains of a lithiated γ-MnO_2 phase and a spinel-related phase[26].

The nature of the X-ray patterns of these CDMO materials is critically dependent on properties of the precursor materials, for example, decomposition temperature, particle size and surface area, and on processing techniques and conditions such as mixing (*eg* hand mixing or ball-milling), oxygen partial pressure, reaction temperature and time of reaction. In an attempt to clarify the structural issues around the different interpretations, a study of the reaction of R-MnO_2 with $LiNO_3$ (Mn:Li = 7:3) at 300 and 380°C was undertaken. The preliminary results of this study have been reported elsewhere[26]. The X-ray diffraction patterns of the products are shown in Fig. 6a and b, together with a typical pattern of a product obtained from the reaction of CMD and $LiNO_3$ for comparison (Fig. 6c).

The product formed at 300°C consists predominantly of a lithiated R-MnO_2 phase (Fig. 6a). It is evident from the smaller shifts of certain peaks to lower 2θ values, for example, the [211], [221] and [420] reflections, that the extent of shear in this product is less than it is in single-phase Li_xMnO_2

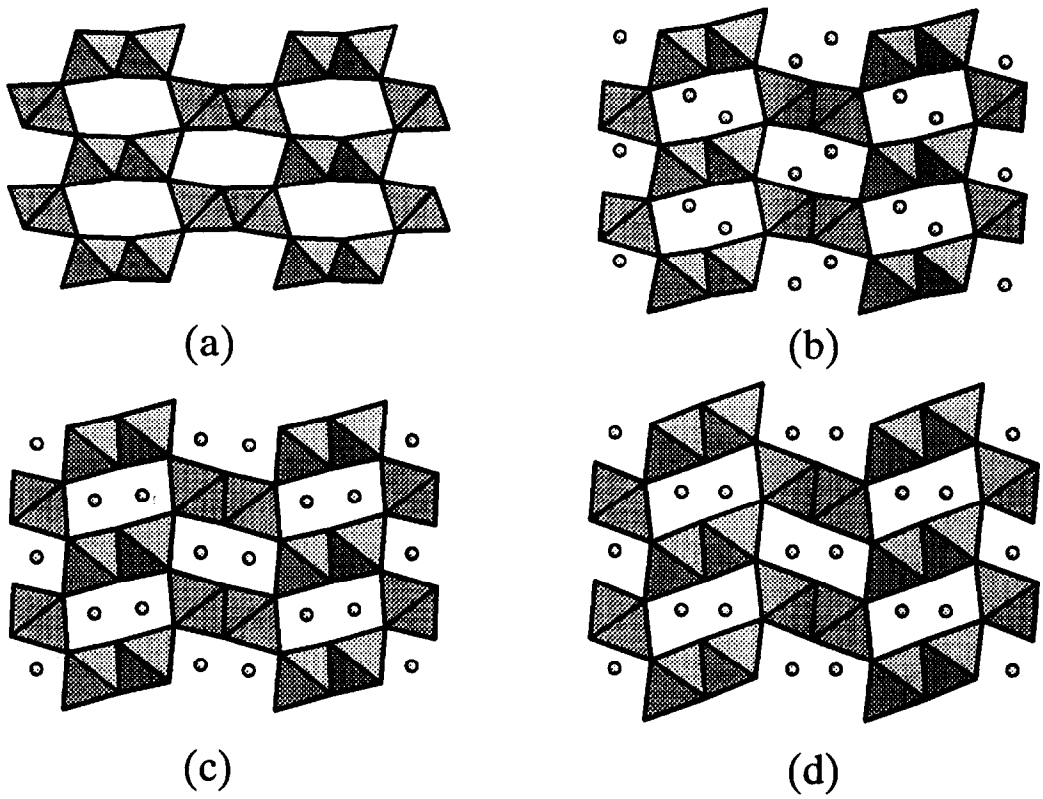

Fig. 5. The structures of: (a) R-MnO_2; (b) $Li_{0.3}MnO_2$; (c) $Li_{0.5}MnO_2$; and (d) $Li_{0.9}MnO_2$ as determined from powder X-ray diffraction data.

products (Fig. 1b–d). Although the [110] peak in Fig. 6a is still clearly resolved at 21°/2θ, there is substantial broadening of this peak. The broadening can be attributed to the reordering of the oxygen ions and the development of a close-packed oxygen array parallel to the *bc* planes; it marks the onset of the spinel [111] reflection at 19.2°/2θ and manganese-ion migration from octahedral sites in the parent R-MnO_2 structure to interstitial octahedral sites.

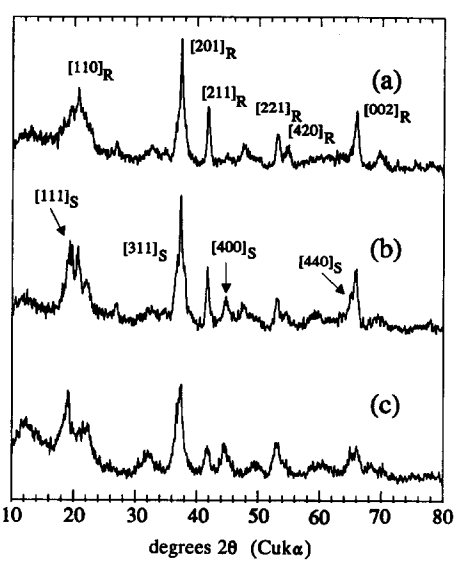

Fig. 6. The powder X-ray diffraction patterns of: (a) the reaction product of R-MnO_2 and $LiNO_3$ (Mn:Li = 7:3) at 300°C; (b) at 380°C; and (c) the reaction product of CMD and LiOH at 370°C. Reflections from the orthorhombic ramsdellite phase are denoted R, those from a cubic spinel phase are denoted S.

It is important to note that in R-MnO_2, as in all the chemically-lithiated products Li_xMnO_2 synthesized at 70°C (Fig. 5a–d), the manganese ions are distributed equally in adjacent layers between the oxygen planes that lie parallel to the *bc* plane. At 300–400°C lithiation induces a shear of the (2 × 1) ramsdellite blocks and a migration of the manganese ions that changes the manganese distribution from the 2:2 ratio in the adjacent layers towards the 3:1 ratio as required by the $[Mn_2]O_4$ framework of the $Li[Mn_2]O_4$ spinel structure. The 3:1 ratio is favored over the 4:0 ratio required by the layered rocksalt Li_2MnO_3 structure, because of the Li:Mn ratio (1:2.33) used in the starting mixture.

The X-ray pattern of the product formed at 380°C (Fig. 6b) is characteristic of intergrown domains consisting of:

(i) a small concentration of R-MnO_2 (probably containing a minor amount of lithium) as evident from the residual [110] peak at 22°/2θ;

(ii) a lithiated R-MnO_2 phase as evident from the [110] peak at 20.5°/2θ; and

(iii) a spinel phase within the system $Li_xMn_{2-z}O_4$ ($0 \leqslant x \leqslant 4/3$, $0 \leqslant z \leqslant 1/3$) as evident from the [111] peak at 19°/2θ.

At 380°C the cubic-close packing of the oxygen ions and the manganese layering in the spinel

domains is better established than it is at 300°C as indicated by the more dominant [111] and [400] peaks at 19°/2θ and 44.5°/2θ, respectively. The spinel phase could be indexed to a cubic unit cell with a lattice parameter of 8.15 Å, which is consistent with the values for other spinel phases within the $Li_xMn_{2-x}O_4$ solid solution system[8]. The X-ray pattern of a product obtained from the reaction of CMD and LiOH at 370°C is shown in Fig. 6c for comparison; it clearly shows the presence of a lithiated γ-MnO_2 phase and a spinel phase. The absence of a strong [110] peak at 20.5°/2θ is significant; it demonstrates the absence of a lithiated-ramsdellite component in the structure. These data therefore suggest that lithiated γ-MnO_2 materials, for example, those derived from typical CMD and EMD products that contain a significant β-MnO_2 component, have a greater tendency to transform directly to the spinel phase.

The migration of manganese from the octahedral sites to interstitial octahedral sites is believed to be the key factor that stabilizes R-MnO_2 and γ-MnO_2 electrodes for rechargeable lithium cells; it is responsible for the creation of stable cubic-close-packed spinel-related domains that are intergrown with the lithiated-ramsdellite phase. These domains suppress the shearing process and the concomitant volume expansion/contraction of the unit cell that accompany lithium insertion/extraction reactions with unstabilized R-MnO_2 and γ-MnO_2 structures.

It has been reported that the typical stoichiometry of lithiated manganese oxide products obtained by reacting CMD (or EMD) with $LiNO_3$ (in a 7:3 molar ratio) at 370°C is $LiMn_3O_6$ ($Li_{0.3}MnO_2$)[24, 25]. The reaction demonstrates that, under specific processing conditions, the MnO_2 precursor is reduced to accommodate the inserted lithium. It is of particular interest to note that $LiMn_3O_6$ products are not single-phase like $Li_{0.3}MnO_2$ prepared at 70°C from R-MnO_2 and LiI (Fig. 1b) despite having the same composition; they have X-ray patterns similar to those of the lithiated MnO_2 products shown in Fig. 6a–c.

The ramsdellite–spinel transformation

When lithiated R-MnO_2 of composition $Li_{0.5}MnO_2$ (Fig. 7a) is heated under vacuum at 300°C for 48 h a transition to a single-phase $LiMn_2O_4$ product (a = 8.250 Å) is observed (Fig. 7b). It is therefore evident that at 70°C there is insufficient energy to displace the manganese ions from the octahedral sites of the R-MnO_2 framework to interstitial sites, whereas the use of higher temperatures assists the diffusion of the manganese cations and the rearrangement of the oxygen ions to ideal cubic-close-packing.

A proposed mechanism for the R-MnO_2–spinel transformation is given in Fig. 8a–c. The driving force behind the transformation is the increase in electrostatic interactions between the inserted Li^+ ions and the manganese ions that reside in neighbouring face-shared octahedra of the hexagonally-close-packed oxygen array. The transformation is described in two stages. The R-MnO_2 structure initially responds to the lithium–manganese interactions by the shear of (2 × 1) R-MnO_2 blocks in the

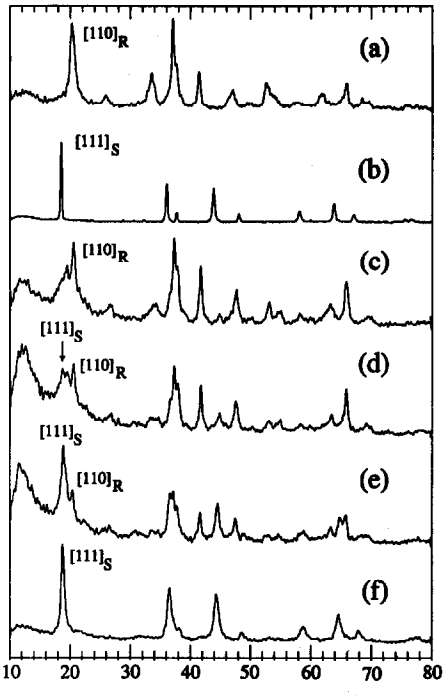

Fig. 7. The powder X-ray diffraction patterns of: (a) $Li_{0.5}MnO_2$ derived from R-MnO_2 and LiI at 70°C; (b) $Li_{0.5}MnO_2$ heated at 300°C under vacuum; (c) $Li_{0.5}MnO_2$ heated at 300°C in air (16 h); (d) (c) heated at 370°C in air (6 h); (e) $Li_{0.5}MnO_2$ heated at 400°C in air (60 h); (f) $Li_2Mn_4O_9$ from the reaction of Li_2CO_3 and $MnCO_3$ at 400°C in air (5 h).

directions shown in Fig. 8a to yield the R-MnO_2 framework in $Li_{0.5}MnO_2$ (Fig. 8b); this is followed by a cooperative displacement of the manganese ions and a second shear to generate the spinel framework (Fig. 8c). In the transformation to spinel it is necessary to displace only one quarter of the manganese ions to achieve the ideal 3:1 layering of the manganese ions in the $[Mn_2]O_4$ spinel framework.

When $Li_{0.5}MnO_2$ is heated in air it oxidizes slowly to form a $Li_{0.5}MnO_{2+y}$ ($0 < y \leqslant 0.25$) product with domains of varying composition and structure; the product ultimately transforms to a defect spinel of composition $LiMn_2O_{4+\delta}$ ($0 < \delta \leqslant 0.5$). The transformation to a defect spinel in air is more sluggish than the transformation under vacuum to the stoichiometric spinel $LiMn_2O_4$. This is to be expected because oxygen must be incorporated into the $LiMn_2O_{4+\delta}$ structure during the transformation.

Figure 7c–e shows the X-ray diffraction patterns of the products formed by heating $Li_{0.5}MnO_2$: (i) at 300°C for 16 h (Fig. 7c); (ii) at 370°C for 6 h (Fig. 7d); and (iii) at 400°C for 60 h (Fig. 7e). Figure 7f shows the X-ray pattern of a typical $LiMn_2O_{4.5}$ ($Li_2Mn_4O_9$) product synthesised from the reaction of $MnCO_3$ and Li_2CO_3 at 400°C[11]. These X-ray patterns show that the transformation of $Li_{0.5}MnO_2$ to the defect spinel $LiMn_2O_{4.5}$ occurs via an intermediate phase indicated, for example, in Fig. 7d by the

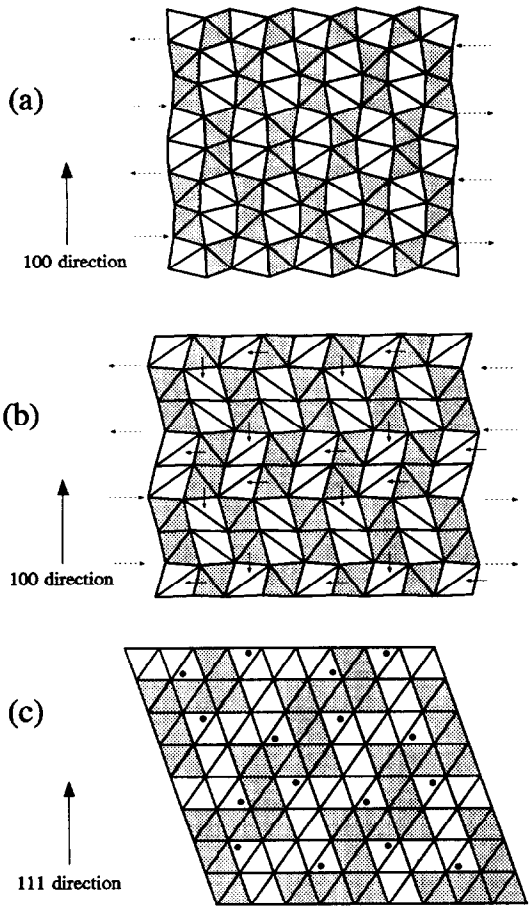

Fig. 8. The R-MnO_2 to spinel transformation. The manganese ions are located in shaded octahedra. (a) R-MnO_2, showing the directions of the initial shear on lithium insertion. (b) The R-MnO_2 framework at a composition $Li_{0.5}MnO_2$. Solid arrows indicate the direction of manganese ion displacement. Broken arrows indicate the direction of shear to generate the cubic close-packed oxygen array. (c) The $[Mn_2]O_4$ framework of $Li[Mn_2]O_4$. Li^+ ions (●) are located in tetrahedral sites in the interstitial space of the framework.

peak at 19.2°/2θ that lies between the [110] lithiated R-MnO_2 peak and the [111] spinel peak; it is attributed to an intergrown structure that separates the lithiated R-MnO_2 phase from the spinel phase. In Fig. 7c the intermediate compound, which is more pronounced than it is in Fig. 7d, could be indexed to a cubic unit cell with $a = 8.082$ Å. Although it has not been possible to refine the structure of the intermediate compound, the parameter value and the intensities of the peaks suggest that it is spinel-like in character. In this respect it is of interest to note that in the spinel system $Li_x[Mn_2]O_4$ ($0 \leqslant x \leqslant 1$) there is a discontinuity in the lattice parameter vs. composition plot at $x \approx 0.25$[27, 28]; the discontinuity has been attributed to the ordering of the Li^+ ions on the tetrahedral sites of the spinel structure. For $0 \leqslant x \leqslant 0.5$, a has been reported to have values between 8.029 and 8.045 Å, whereas for $0.5 \leqslant x \leqslant 1.0$, a varies from 8.142 to 8.248 Å. By analogy, therefore, it seems possible that the transformation of $Li_{0.5}MnO_2$–$LiMn_2O_{4.5}$ takes place via a spinel-like intermediate which is lithium deficient. It should also be noted in Fig. 7c–e that the lithiated R-MnO_2 peak [110] shifts to lower 2θ as the heating temperature (in air) is raised; it indicates an expansion of the unit cell and a concomitant oxidation of the lithiated R-MnO_2 phase to $Li_{0.5}MnO_{2+\delta'}$ ($0 < \delta' \leqslant 0.25$).

The data provided above demonstrate that the $[Mn_{2-z}]O_4$ ($0 \leqslant z \leqslant 1/3$) spinel framework plays a key role in the synthesis of highly crystalline R-MnO_2 products. When $Li_2Mn_4O_9$ is used as the spinel precursor, R-MnO_2 is obtained by leaching Li_2O from the spinel structure according to the reaction:

$$Li_2Mn_4O_9 \underset{300-400°C}{\overset{95°C,\ acid}{\rightleftharpoons}} 4MnO_2 + Li_2O.$$

The spinel–ramsdellite transition is reversible but higher temperatures and long reaction times are required to allow the reaction to go to completion in the reverse direction. The reversibility of this system is consistent with reports that spinel structures in the $Li_xMn_{2-z}O_4$ system ($0 \leqslant x \leqslant 4/3$, $0 \leqslant z \leqslant 1/3$) are favoured over other structure types when synthesized in the temperature range 300–400°C, and particularly when the Li:Mn ratio falls within the range 1:1.2 to 1:2.0[26].

Electrochemical characterization of R-MnO_2

The voltage profile of a Li/R-MnO_2 cell is shown in Fig. 9. On closed circuit the R-MnO_2 electrode delivers a capacity of 220 mAh g^{-1} to a 2 V limit, which is 71% of the theoretical capacity (308 mAh g^{-1}). The open-circuit voltage profile shows that discharge occurs in three distinct stages to a composition $LiMnO_2$ with interruptions in the profile at $x \approx 0.3$ and $x \approx 0.9$. In view of the structural information given above, the first two stages can be attributed to the following processes:

1. $0 \leqslant x \leqslant 0.3$: Insertion of lithium into an essentially hexagonally-close-packed R-MnO_2 structure. This finding is consistent with X-ray data reported by Ohzuku *et al.* for heat-treated EMD samples that show the onset of structural changes in Li_xMnO_2 samples at $x \approx 0.3$[4, 5];

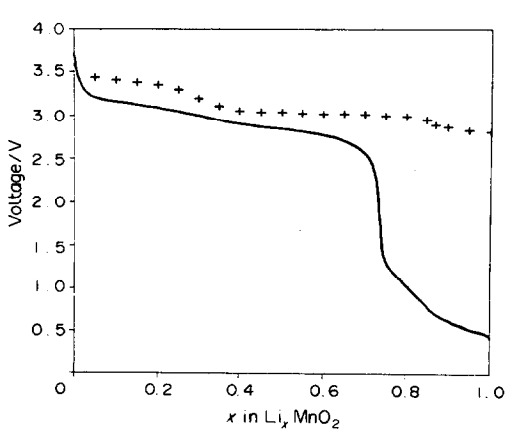

Fig. 9. The open-circuit-voltage (+) and closed-circuit-voltage (——) profiles of a Li/R-MnO_2 cell (cd = 0.4 mA).

2. $0.3 \leqslant x \leqslant 0.9$: Insertion of lithium into an R-MnO_2 framework structure in which the packing of the oxygens is essentially ABACABAC.

The process at the end of discharge ($0.9 \leqslant x \leqslant 1.0$) is not yet clearly understood; it can possibly be attributed to lithium insertion into an R-MnO_2 framework structure in which the packing is ABCABC. In this event the end product is a rocksalt phase $LiMnO_2$ in which the close-packed oxygen array is distorted from ideal cubic-close-packing by the Jahn–Teller Mn^{3+} (d^4) ions.

Preliminary investigations of the rechargeability of room temperature Li/R-MnO_2 cells indicate that the R-MnO_2 electrode does not cycle well on deep discharge (Fig. 10). The capacity drops from an initial 230 mAh g^{-1} to 160 mAh g^{-1} on the second discharge; thereafter the capacity declines steadily to reach a value of 115 mAh g^{-1} after 10 cycles. The capacity loss can be attributed to the large expansion and contraction of the unit cell on deep discharge and recharge, and to concomitant structural modifications that occur on cycling lithium between an essentially hexagonally-close-packed structure and one which has cubic-close-packed character. If the cycling regime is controlled to allow the electrode to operate only on the second plateau ($0.3 \leqslant x \leqslant 0.9$) an improved capacity retention can be expected; such an electrode has a theoretical capacity of 181 mAh g^{-1}. This observation is in good agreement with the performance of EMD electrodes heated at 250°C which, after an initial discharge capacity of 220 mAh g^{-1}, deliver steady capacities of 150 mAh g^{-1} when cells are cycled between 3.8 and 2.0 V at low current rates (0.17 mA cm^{-2})[5].

The significant decrease in the reduction peak on the second cycle of a cyclic voltammogram confirms the capacity loss observed in the Li/R-MnO_2 cell (Fig. 11). On the anodic scan, the voltammogram shows a two-stage process for lithium extraction that corresponds to the first two reduction processes observed on the OCV vs. composition plot in Fig. 9. The first anodic peak at 3.6 V is therefore attributed to the removal of lithium from the intergrown hexagonal/cubic-close-packed anion array (ABACABAC); the second anodic peak at 4.1 V is attributed to the further removal of Li^+ ions from the structure and a concomitant shear to regenerate the original hexagonally-close-packed structure.

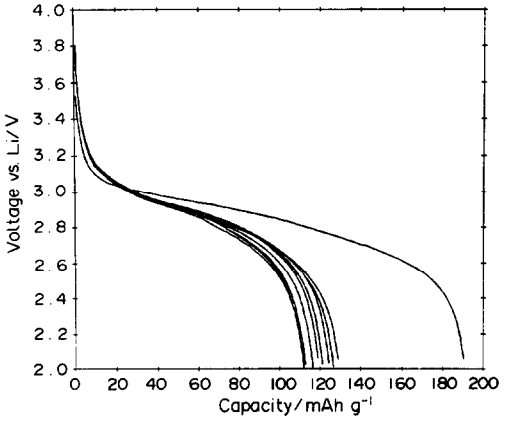

Fig. 10. The first ten discharge cycles from a Li/R-MnO_2 cell (cd = 0.4 mA).

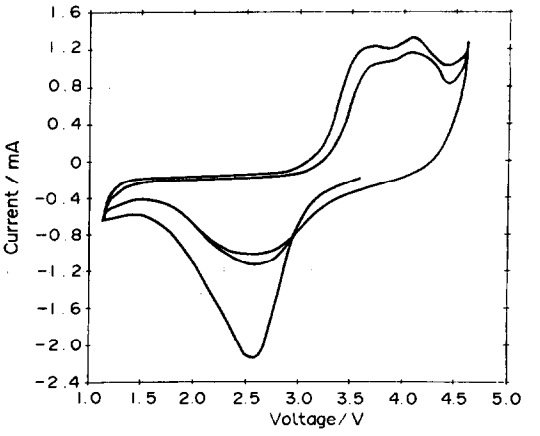

Fig. 11. The cyclic voltammogram of a Li/R-MnO_2 cell (sweep rate = 0.2 mV s^{-1}).

CONCLUSIONS

Lithiation of R-MnO_2 has been demonstrated by chemical and electrochemical methods. The stability of R-MnO_2 electrodes and rechargeability of Li/R-MnO_2 cells (and by inference Li/γ-MnO_2 cells) are dependent on a Li_xMnO_2 structure with domains that are characterized by an oxygen array with cubic-close packed character. When R-MnO_2 is stabilized by reaction with a lithium salt (Mn:Li = 7:3) at 300–400°C, the displacement of manganese ions from the octahedral sites of the R-MnO_2 framework into interstitial octahedral sites provides cubic-close-packed domains with spinel character that coexist with domains of a lithiated ramsdellite phase; the concentration of the spinel domains in the intergrown structure increases as the reaction temperature is raised.

REFERENCES

1. T. Ohzuku, M. Kitagawa, K. Sawai and T. Hirai, *J. electrochem. Soc.* **138**, 360 (1991).
2. M. H. Rossouw, D. C. Liles and M. M. Thackeray, *Mat. Res. Bull.* **27**, 221 (1992).
3. M. A. Humbert, Ph. Biensan, M. Broussely, A. Lecerf, A. Dollé and H. Ladhily, *Ext. Abstr. III-C-06*, 6th Int. Meeting on Lithium Batteries, Munster, Germany, 10–15 May (1992).
4. T. Ohzuku, M. Kitagawa and T. Hirai, *J. electrochem. Soc.* **136**, 3169 (1989).
5. T. Ohzuku, M. Kitagawa and T. Hirai, *J. electrochem. Soc.* **137**, 40 (1990).
6. M. H. Rossouw and M. M. Thackeray, *Mat. Res. Bull.* **26**, 463 (1991).
7. T. Ohzuku, A. Ueda and T. Hirai, *Chem. Express* **7**, 193 (1992).
8. M. M. Thackeraray, A. de Kock, M. H. Rossouw, D. C. Liles, R. Bittihn and D. Hoge, *J. electrochem. Soc.* **139**, 363 (1992).

9. J. M. Tarascon, E. Wang, F. K. Shokoohi, W. R. McKinnon and S. Colson, *J. electrochem. Soc.* **138,** 2859 (1991).
10. V. Manev, A. Momchilov, A. Nassalevska and A. Kozawa, *Ext. Abstr. III-B-11*, 6th Int. Meeting on Lithium Batteries, Munster, Germany, 10–15 May (1992).
11. A. de Kock, M. H. Rossouw, L. A. de Picciotto, M. M. Thackeray, W. I. F. David and R. M. Ibberson, *Mat. Res. Bull.* **25,** 657 (1990).
12. T. Nohma, T. Saito, N. Furukawa and H. Ikeda, *J. Power Sources* **26,** 389 (1989).
13. T. Nohma, Y. Yamamoto, I. Nakane and N. Furukawa, *J. Power Sources* **39,** 51 (1992).
14. M. Ripert, J. Pannetier, Y. Chabre and C. Poinsignon, *Mat. Res. Soc. Proc.* **210,** 359 (1991).
15. Y. Chabre and M. Ripert, *Mat. Res. Soc. Proc.* **210,** 367 (1991).
16. D. W. Murphy, F. J. DiSalvo, J. N. Carides and J. V. Waszczak, *Mat. Res. Bull.* **13,** 1395 (1978).
17. W. I. F. David, M. M. Thackeraray, P. G. Bruce and J. B. Goodenough, *Mat. Res. Bull.* **19,** 99 (1984).
18. J. Schneider, *IUCr Int. Workshop on the Rietveld Method*, Pelten (1989).
19. P. J. Brown and J. C. Matthewman, Rutherford Appleton Laboratory Report, RAL 87-010, May (1987).
20. W. I. F. David and R. M. Ibberson, Rutherford Appleton Laboratory Report. In preparation.
21. JCPDS Powder Diffraction File 7-222.
22. L. Li and G. Pistoia, *Solid State Ionics* **47,** 231 (1991).
23. L. Li and G. Pistoia, *Solid State Ionics* **47,** 241 (1991).
24. M. Yoshio, S. Inoue, G. Piao and H. Nakamura, *Prog. Batts Sol. Cell* **9,** 205 (1990).
25. M. Yoshio, H. Nakamura and H. Noguchi, *Prog. Batts Batt. Mats* **10,** 23 (1991).
26. M. M. Thackeray, M. H. Rossouw, A. de Kock, A. de la Harpe, R. J. Gummow, K. Pearce and D. C. Liles, *J. Power Sources*, In press (1992).
27. W. I. F. David, M. M. Thackeray, L. A. de Picciotto and J. B. Goodenough, *J. Solid State Chem.* **67,** 316 (1987).
28. T. Ohzuku, M. Kitagawa and T. Hirai, *J. electrochem. Soc.* **137,** 769 (1990).